Fire Safety Journal 129 (2022) 103569

Contents lists available at ScienceDirect

Fire Safety Journal

journal homepage: www.elsevier.com/locate/firesaf

The controlling mechanisms of horizontal flame spread over thick rods in upward cross flow

Chuanjia Wu [a,b], Feng Zhu [a,*], Shuangfeng Wang [a,b,c]

[a] Key Laboratory of Microgravity, Institute of Mechanics, Chinese Academy of Sciences, Beijing, 100190, China
[b] School of Engineering Science, University of Chinese Academy of Sciences, Beijing, 100049, China
[c] State Key Laboratory of High-Temperature Gas Dynamics, Chinese Academy of Sciences, Beijing, 100190, China

ARTICLE INFO

Keywords:
Stretch rate
Flame spread
Regression
Flammability
Cylinder

ABSTRACT

This work studies the flame spread over horizontal thick PMMA (polymethyl methacrylate) rods with three radii under different oxygen concentrations and upward cross flow velocities. The flame spread rate and the limit oxygen concentration are measured. Far away from the extinction limit, the flame spread rate increases with the flow velocity but decreases with radius. Near the extinction limit, the flame spread rate is insensitive to the flow velocity and radius. The flame spread rate can be correlated by the stretch rate, and it is found that the flame spread rates for different radii are close at the same stretch rate. A scaling analysis shows that the flame spread rates are approximately square-root dependent on the stretch rate. Prior to the extinction, the flame has entered the regressive burning regime where the flame leading edge will not spread forwardly but continuously retreat. The flame extinction is dependent on the local stretch rate and in-depth heat conduction. For a given radius, the limit oxygen concentration increases with the stretch rate. For a given stretch rate, the smaller cylinder can sustain at lower oxygen concentration due to the less solid-phase heat loss.

1. Introduction

Flame spread over the solid combustible surface is of great interest for fire safety research, due to its influence on the initial fire development and heat release rate [1]. Opposed and concurrent flame spread mechanisms over solid fuels have been extensively investigated for several decades (e.g., the reviews of Fernandez-Pello et al. [2], Quintiere et al. [3], and Gollner et al. [4]), which result in a significant contribution to the development of fire research. Generally, the classification of opposed and concurrent flame spread is based on the relative direction between flame spread and ambient flow. The flame spreads in the reverse direction against the flow in the former case and the same direction of flow in the latter case [2]. Extended studies of flame spread over inclined fuel samples were performed [5–9], and the flame spread behaviors in those studies are similar to opposed or concurrent flame spread. However, the direction of flame spread and the gas flow is not always collinear. Typically, in the ceiling or floor flame spread, the direction of buoyant flow is perpendicular to that of flame spread. The variation of the flow direction can change the flame standoff distance and alter the heat flux from the flame to the fuel, which in turn affects the gas-phase reaction and flame spread behavior [10,11]. Therefore, it is necessary to investigate flame spread behavior in more complex flow conditions. Some researchers have focused on this problem. For example, Tizon et al. [12] studied the flame spread process under oblique forced flow in absence of gravity. Zhao et al. [13] conducted lateral flame spread over PMMA slab in forced flow and they developed a heat transfer model based on the laminar diffusion flame theory to predict the flame spread rate. Higuera and Linan [14–16] have investigated the horizontal flame spread behavior over PMMA cylinders in buoyant flow and the absence of gravity environments.

To further study the flame spread behavior in a mixed convection flow, the horizontal flame spread over thick rods under upward forced flow is focused on in this work. The flame spread configuration, in this case, is similar to the studies about the stagnation-point diffusion flame [17–20]. The flame in the non-uniform flow field is subjected to the effect of the stretch rate. The numerical model about the stagnation-point diffusion flame [17] showed that the flame characteristics, e.g. extinction boundary, and mass burning rate, are almost identical at the same mixed stretch rate. For a spreading flame, Wichman [21] and Hossain et al. [22] used the flame stretch theory to explain flame spread behavior. Wichman [21] proposed a theoretical model to describe the flame spread rate in the flow with a linear velocity gradient.

* Corresponding author.
E-mail address: zhufeng@imech.ac.cn (F. Zhu).

https://doi.org/10.1016/j.firesaf.2022.103569
Received 10 November 2021; Received in revised form 27 January 2022; Accepted 16 March 2022
Available online 18 March 2022

This theory shows that the flame stretch rate has a greater influence on flame spread rate than flow velocity. Hossain et al. [22] conducted flame spread experiments in narrow channel apparatus and compared the differences between the flame spread rate in the buoyancy-suppressed and fully developed environment [23]. They found that the two sets of flame spread rates are in great agreement when their stretch rates are close. These results suggest that the stretch rate is a potential factor to characterize the flame spread behavior.

The present work aims to investigate the effects of flow velocity, fuel radius, and stretch rate on the horizontal flame-spread and extinction behavior over thick rods in upward cross flow as well as the controlling mechanisms. Three PMMA cylinders with radii of 10, 20, 50 mm are used to perform the experiments at various oxygen concentrations. The influences of stretch rate on flame spread and extinction behavior are quantified and discussed.

2. Experimental apparatus

Fig. 1 shows the schematic of experimental apparatus designed to conduct flame spread experiments over horizontal cylindrical PMMA. The vertically oriented flow tunnel has an outer diameter of 100 mm, an inner diameter of 90 mm, and a height of 530 mm, which is the same as in Reference [24,25]. It was composed of a quartz glass tube and a flow homogenizer section which is full of aluminum honeycomb and glass beads to smooth flow. The ambient atmosphere was O_2/N_2 mixture which can be achieved by mixing air supplied from the compressor with N_2 or O_2 supplied from gas bottles. The gas flow velocity and oxygen concentration were adjusted by two mass flow controllers (Alicat Scientific, type MC) which allow the mixture with a prescribed oxygen concentration (X_{O2}) between 15% and 25% at flow velocities (V_g) from 0 to 60 cm/s. The flow rate and oxygen concentration were measured using a hot-wire anemometer and a fuel gas analyzer (TESTO 350) respectively at the outlet of the flow tunnel. A digital video camera (Nikon D7200, 25fps) with a resolution of 1920 by 1080 was employed to record the burning and extinction process from the front view.

The PMMA samples with radii of 10, 20, 50 mm, and a constant length of 70 mm were used in this experiment. For the sample with the largest radius ($r = 50$ mm), it was cut as a 70 mm × 70 mm × 12 mm slab and then heated at 160 °C for about 90 min until it was pliable [19]. The hot sample was immediately placed in a cylindrical steel mold and press the sample to the wall of the mold to have the desired radius. The other two samples are solid cylinders that are cut from the cast PMMA slab. These samples are all thermally thick fuels, for the fact that the length of the heated layer is smaller than the radius of the sample. The sample was placed 15 mm above the center of the flow tunnel which acted as a nozzle. To verify the uniformity of the flow field around the sample, the velocity profile at the outlet of the flow tunnel was measured by a hot-wire anemometer, and the velocity profiles are provided in the Fig. A1.

When performing the flame spread experiment, one end of the sample is ignited by a torch in the environment with preset oxygen concentration and flow velocity. The flammability tests have little difference compared to the flame spread experiments. To preclude the effect of ignition on flame extinction limit, the sample is firstly ignited in the air. The oxygen concentration is decreased by 1% at 30 s intervals when $X_{O2} \geq 19\%$. To obtain a more accurate flammability boundary, the oxygen concentration is decreased slowly by 0.5% at the same intervals when $X_{O2} < 19\%$ until the flame is extinct. To reduce random errors, each test was repeated at least three times. The relative errors of oxygen concentration are about ±0.2%. The precision of the gas flow velocities in the forced flow experiments is about ±5%. The uncertainty on the measured flame spread rate is mainly due to the ambiguity of the flame leading edge.

3. Results

3.1. Flame spread and fuel regression behaviors

Fig. 2 shows the horizontal spreading flame with radii of 10, 20, and 50 mm in the air. It is seen that the flame is yellowish when $r \leq 20$ mm, indicating the soot content is high for the present experiments. With the increase of radius, the flame becomes dim. For $r = 50$ mm, the flame is weak and blue after the ignition. As the flame spread forwardly, the middle part of the flame becomes yellow, but the leading edge and the tail of the flame are always blue during the test. Fig. 3 shows the horizontal spreading flame with a radius of 10 mm at various upward cross flow velocities at $X_{O2} = 18\%$. Under low oxygen concentration, there is no significant change in the flame appearance compared with $X_{O2} = 21\%$, as shown in Fig. 3(a). However, the spreading flame will transit to fuel regression prior to the extinction with the increased oxidizer flow velocity. Fig. 3(b) shows the photographic sequence of fuel regression with a radius of 10 mm PMMA rod at a flow velocity of 40 cm/s. When the flame entered the regressive burning regime, the flame front will not spread forward but continuously retreat until the flame beneath the

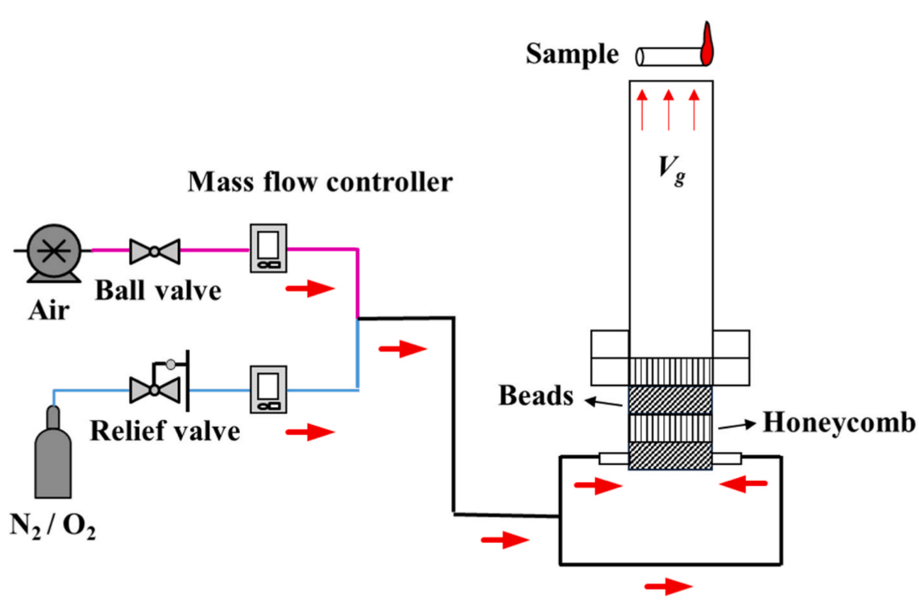

Fig. 1. Schematic of the experimental setup.

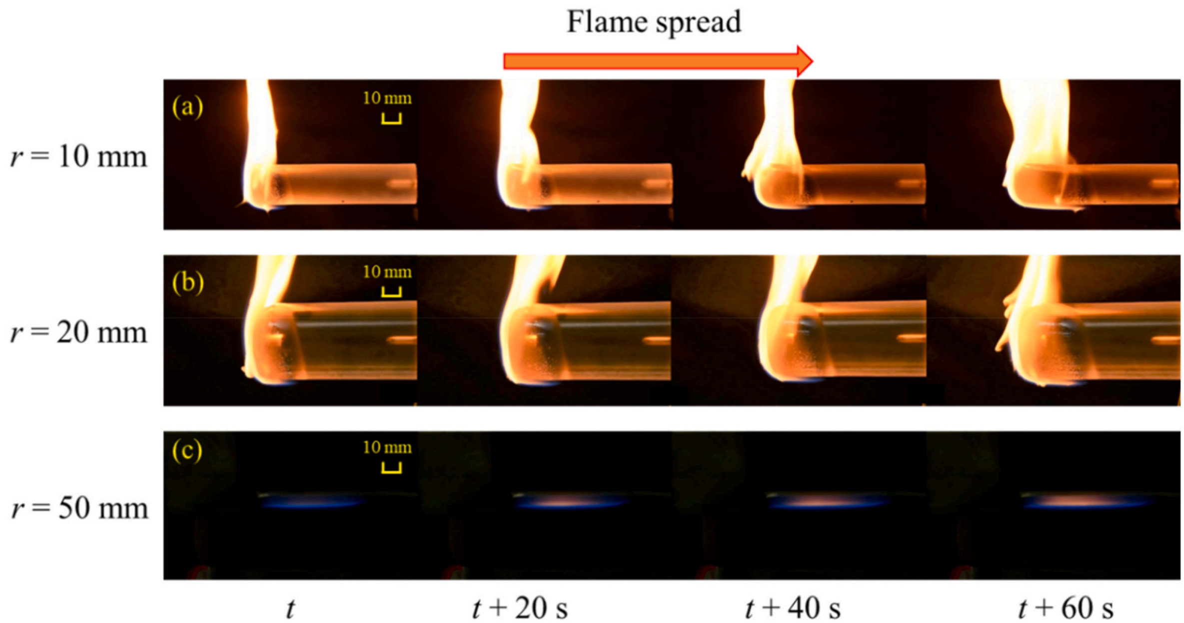

Fig. 2. Images of horizontal flame spread with radii of 10, 20, 50 mm in the air with buoyant flow.

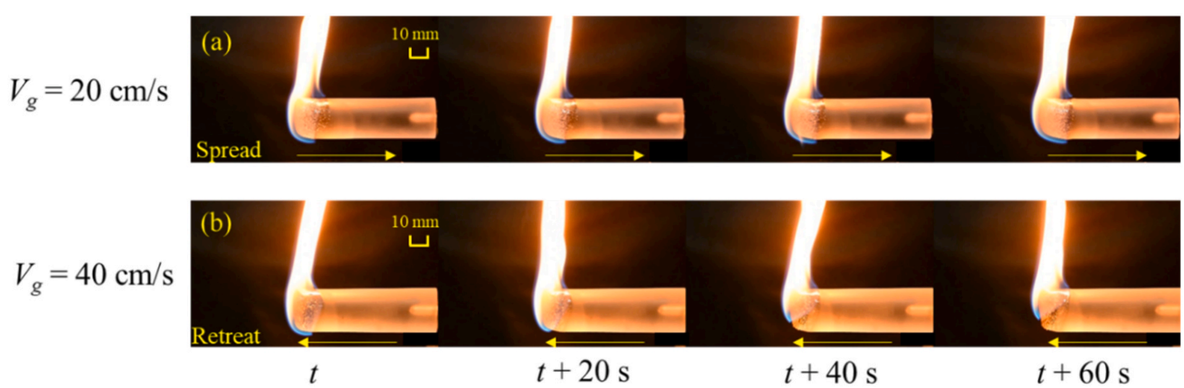

Fig. 3. Images of horizontal flame spread and regression with the radius of 10 mm at the gas velocity of 20, and 40 cm/s under $X_{O2} = 18\%$.

cylinder is extinct. The flame leading edge is locally blown off because of the slow chemical reaction rate and the flame moves to the back surface of the sample to sustain the burning. However, the flame can still sustain and even spread along the rear surface of the PMMA cylinders. The flame will be totally blown off when the upward cross flow reaches a critical velocity. Moreover, as the oxygen concentration increased to 21%, the sample with a smaller radius of 10 mm regresses when the flow velocity is greater than 40 cm/s, and the critical flow velocity for fuel regression increases with the radius which is in agreement with that for downward burning conditions [27]. At 18% O_2, the critical velocity is about 30 and 40 cm/s for a sample with a radius of 50 mm and 10 mm respectively. The fuel-regression behaviors can be also observed in reduced pressure, lower oxygen concentration and microgravity (low velocity) environments [27] where the finite rate chemical kinematic dominates the flame behavior. It can be inferred that the regressive burning behavior at $X_{O2} = 25\%$ will occur at a larger flow velocity although not observed in this work.

Fig. 4 plots the flammability boundary for flames spreading over PMMA under upward cross flow. It should be noted that the extinction limit refers to the oxygen concentration and flow velocity at which the flame is totally extinguished. It is seen that the limit oxygen concentration increases with the gas flow velocity but decreases with the diameter.

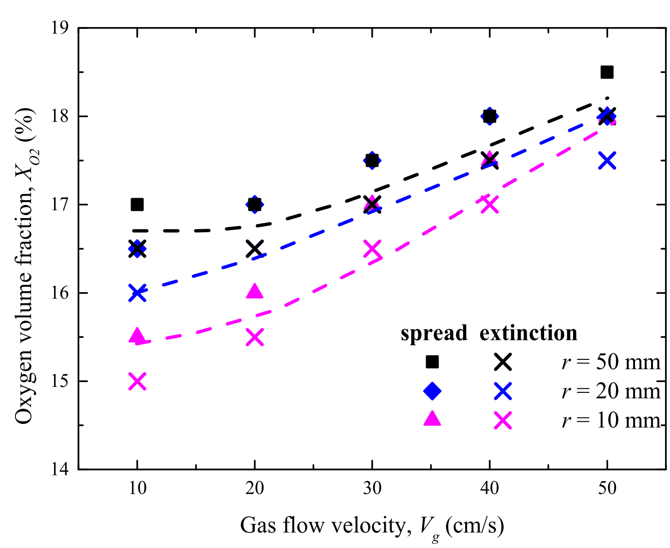

Fig. 4. Extinction boundary using oxygen volume fraction and gas flow velocity as coordinates.

3.2. Flame spread rate

The variations of flame spread rate over the bottom surface of the PMMA rods as a function of gas flow velocity, together with the data of downward flame spread rate, are shown in Fig. 5 for several oxygen volume fractions. The flame spread rate is almost a constant after the ignition indicating that horizontal flame spread is in a steady-state and the time evolution of flame leading-edge position is provided in Fig. A2. It is seen that at high oxygen concentrations ($X_{O2} \geq 21\%$), the flame spread rate almost increases monotonically as the gas flow velocity increases, as shown in Fig. 5(a) and (b). Another observation is that, at a given flow velocity, the flame spread rate decreases with the increased sample radius. One possible factor to consider that could explain this variation trend is the curvature effect. For the larger cylinder, the heat transfer from the flame to the solid fuel is decreased due to the curvature effect, and the temperature of the solid phase increases slower because of the larger heat inertia [26]. Also shown in Fig. 5 is the data on downward flame spread rate over PMMA rods, which were measured previously in the same apparatus used in this work [24,25]. Comparatively, for downward spread flame, the data exhibit a different trend as the flow velocity increases, they are independent of the forced flow velocity when it is smaller than the buoyancy-induced flow (~30 cm/s) [24,25], under which the buoyant flow overwhelms the forced flow and controls the downward flame spread. At a low oxygen concentration ($X_{O2} = 18\%$, Fig. 5(c)), the flame spread rate appears practically independent of the flow velocity and radius. This variation may be caused by the finite chemical reaction rate caused by the low oxygen concentration.

4. Discussion

4.1. Scaling analysis on flame spread

When the flame spreads in the non-uniform flow, the flame sheet is subjected to strain and curvature effects [28], and it will lead to the change in the flame area which can be described by stretch rate. In the classical flame spread theory, an Oseen flow approximation is used [29], and the effect of the stretch rate is neglected. However, the flame spread behavior in this work is mainly affected by the combination of buoyant and forced flow stretch rates. The buoyant flow stretch rate a_b is given by Ref. [17]:

$$a_b = \sqrt{\frac{T^* - T_\infty}{T^*}\frac{g}{r}} \tag{1}$$

where T^* is the reference flame temperature (900 K [30]) that is an average temperature between the pyrolysis (T_v) and the flame temperature (T_f), T_∞ is the ambient temperature (300 K) and g is gravity acceleration (9.81 m/s^2). The forced flow stretch rate a_f for the cylindrical fuel is given as $a_f = 3V_g/2r$. The mixed flow stretch rate a is expressed as:

$$a = \sqrt{a_b^2 + a_f^2} \tag{2}$$

For flame spread over horizontal cylindrical fuels in upward flow, the characteristic length in solid and gas phase as shown in Fig. 6 are expressed as [31]:

$$\begin{aligned} L_{gx} \sim L_{sx} \sim \alpha_g/V_f \\ L_{gy} \sim \sqrt{\alpha_g/a} \\ L_{sy} \sim \sqrt{\alpha_s L_{sx}/V_f} \sim \sqrt{\alpha_s \alpha_g/V_f} \end{aligned} \tag{3}$$

where α is the thermal diffusivity, the subscripts "s" and "g" represent the solid and the gas phase, respectively. For thermally thick fuel, penetration depth τ_h is smaller than the sample radius which can be estimated by L_{sy}, i.e. $\tau_h \sim L_{sy} \sim \sqrt{\alpha_s \alpha_g}/V_f$.

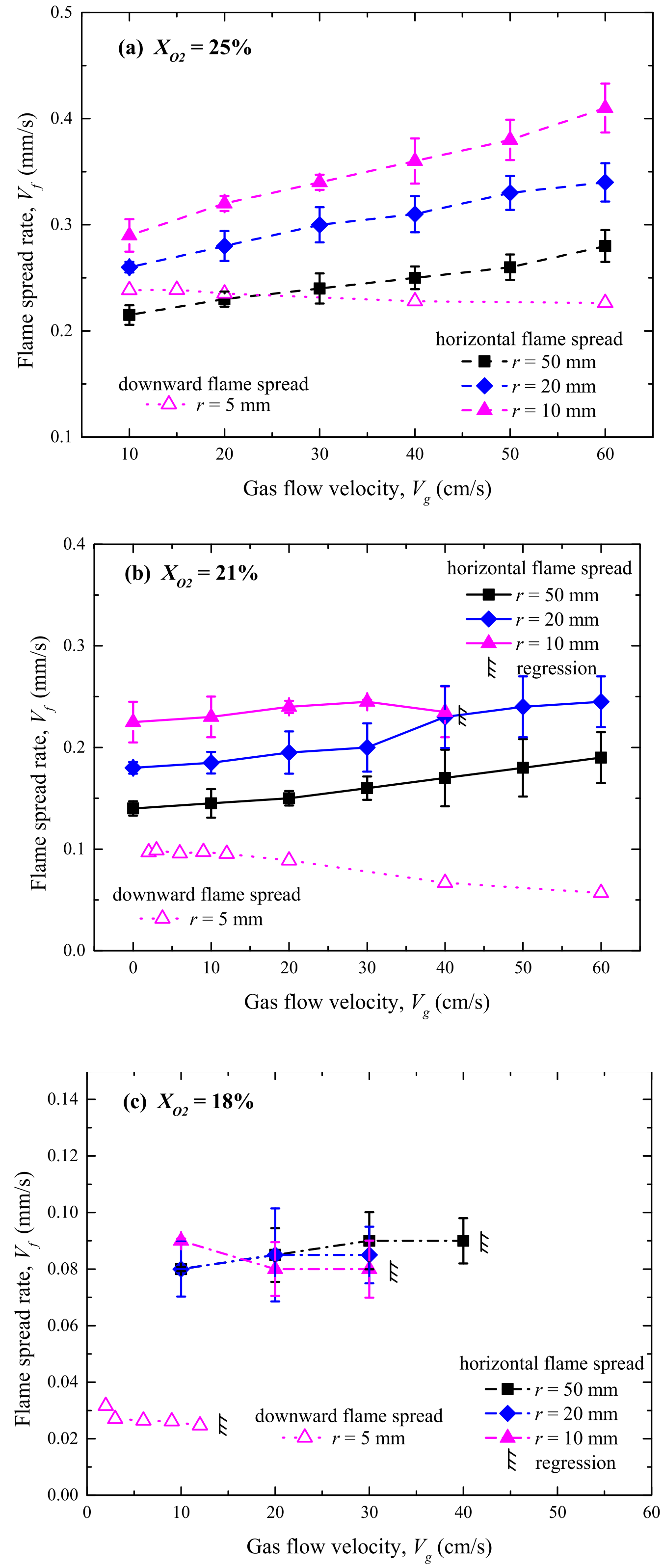

Fig. 5. Flame spread rates as a function of gas flow velocity under (a) X_{O2} = 25%, (b) X_{O2} = 21%, and (c) X_{O2} = 18%. The data of downward flame spread rates come from References [24,25].

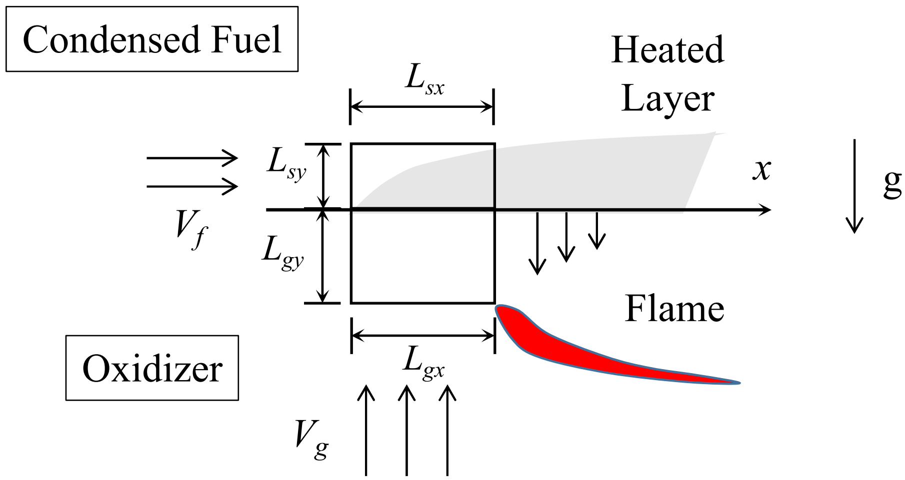

Fig. 6. Solid and gas phase control volumes at the flame leading edge for a cylindrical fuel.

Considering that the flame is almost parallel to the solid fuel, the view factor from the flame to the control volume is small. Therefore, the flame radiative heat flux to the solid fuel is neglected. In the thermally controlled flame spread, the surface radiation and gas phase kinetics can also be neglected, and an energy balance for the solid phase control volume of Fig. 6 yields that:

$$V_f\rho_s c_s(T_v - T_\infty)\pi(r^2 - (r-\tau_h)^2) \sim \frac{k_g(T_f - T_v)}{L_{gy}}L_{gx}f2\pi r \tag{4}$$

$$f = \frac{c\frac{L_{gx}}{r}}{\ln(1 + c\frac{L_{gx}}{r})} \tag{5}$$

where ρ_s and c_s are the density and specific heat of the solid phase, k_g is the heat conductivity of the gas phase, f is the heat transfer factor that accounts for the fuel curvature effect [26], c is a constant varied with flow conditions. Simplify the above equations, the flame spread rate can be expressed as:

$$V_f \sim f\left(1 - \frac{\tau_h}{2r}\right)^{-1}\frac{k_g}{\rho_s c_s \tau_h}\left(\frac{T_f - T_v}{T_v - T_\infty}\right)\frac{L_{gx}}{L_{gy}} \tag{6}$$

if $L_{gx} \ll r$ and $\tau_h \ll r$, the flame spread rate can be further simplified as:

$$V_f \sim \frac{k_g}{(k_s\rho_s c_s)^{1/2}}\left(\frac{T_f - T_v}{T_v - T_\infty}\right)\sqrt{a} \tag{7}$$

Assuming the physical properties are constants, the simplified relationship between the flame spread rate and the stretch rate is obtained, i.e. $V_f \sim \sqrt{a}$. This scaling analysis indicates that the flame spread rate in the thermal regime is dependent on the stretch rate, which is similar to the result of opposed flame spread in a linear gradient flow [21].

In Fig. 7, the flame spread rate results shown in Fig. 5 are replotted as a function of mixed-flow stretch rate for various oxygen concentrations. It is evident that the flame spread rate with different radii and flow velocities are close if their stretch rates are the same. This result is similar to the stagnation-point diffusion flame theory where the fundamental flame characteristics, such as mass burning rate, maximum temperature, and flammability boundary, are almost identical for the same stretch rate [17]. Near the flame extinction limit, the flame spread rates have little change with the stretch rate. The flame spread rates are increased with the stretch rate when $X_{O2} > 21\%$. By fitting the results, it is found that the flame spread rates have a power-law fitting function with stretch rate, $V_f \sim a^n$. The power-law exponent n is 0.32 at $X_{O2} = 21\%$ and 0.26 at $X_{O2} = 25\%$, which is approximate to the predicted 0.5. The deviation from the theoretical prediction is probably due to ignoring the curvature effect in Eq. (6), surface and flame radiation in Eq. (4).

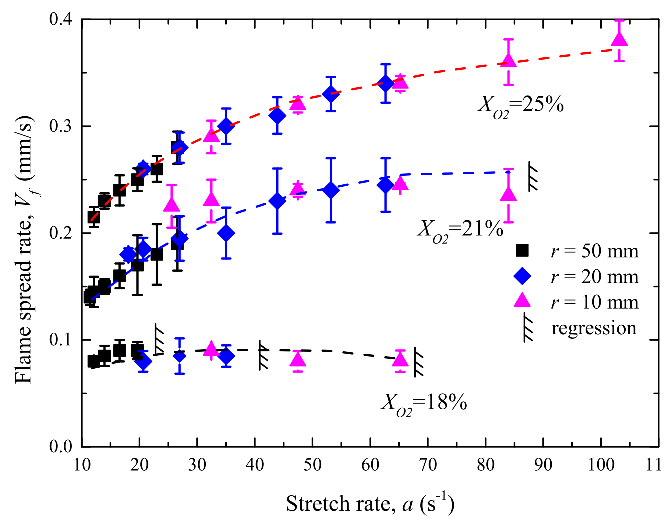

Fig. 7. Flame spread rates as a function of mixed-flow stretch rate a.

Notably, the critical stretch rates for occurring fuel regression with different radii are not the same and vary with fuel size.

4.2. The role of stretch rate on flammability boundary

Fig. 8 shows the flammability boundary as a function of stretch rate. It is seen that the limit oxygen concentrations for all the rods are increased with the stretch rate during the tests and the smaller cylinder has a lower limit for a given stretch rate. The flammability boundary with various radii is different even if the stretch rate is the same, implying that the flammability of the fuel cannot be determined only by the stretch rate.

Near the extinction limit, the flame entered regressive burning regime and $V_f \sim 0$. The energy balance at the surface is established which can be expressed as [32]:

$$\dot{q}''_{f,c} + \dot{q}''_{f,r} = \dot{m}''L_v + \dot{q}''_{s,c} + \dot{q}''_{s,r} \tag{8}$$

where the subscripts "f" and "s" represent the heat flux from flame and solid phase, "c" and "r" represent the conduction and radiation. $\dot{m}''$ is the mass burning rate, L_v is the latent heat. During the flame spread process, $\dot{q}''_{s,c}$ is varied with the fuel radius and the burning time, which is different from the previous studies about the stagnation-point diffusion flame where the ice bath is used to control the solid heat loss [19]. Besides, the

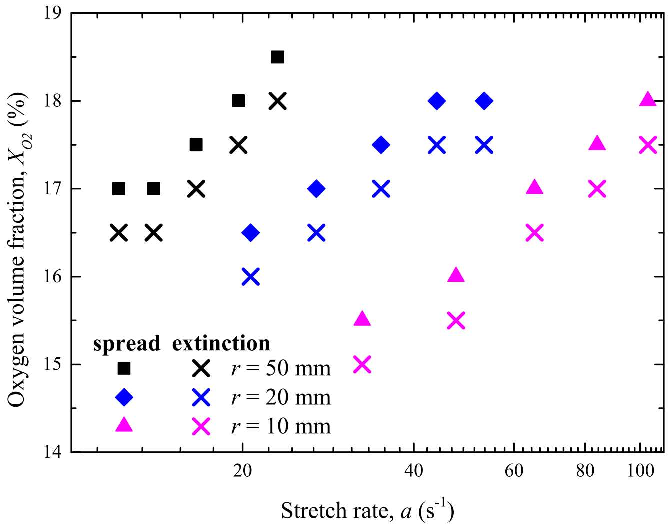

Fig. 8. Extinction boundary using oxygen volume fraction and mixed-flow stretch rate a as coordinates.

distribution $\dot{q}''_{s,c}$ along the length direction may change due to the variation of the temperature gradient inside the solid. For the smaller cylinder, it is faster to heat the solid phase due to its smaller thermal inertia at the same burning time. Similar results are also found in the study of spherical solid fuel-burning behavior [33]. Therefore, the conductive cooling effect decreases slower compared to a larger cylinder. The numerical simulation shows that the larger ratio between $\dot{q}''_{s,c}$ and $\dot{q}''_{f,c}$ will lead to flame extinction, even if at the same stretch rate [34]. Due to the smaller heat loss, the net heat flux is larger for the smaller cylinder which can sustain the flame burning at lower oxygen concentration. Overall, it is implied that the flame extinction limit is affected by the combined effect of stretch rate and heat loss into the solid interior. To further illustrate the mechanism of extinction, a sophisticated numerical model or a precise experiment to measure the dominant heat transfer flux is needed in the future.

5. Conclusions

A series of flame spread experiments over horizontal thick PMMA cylinders in upward cross flow are conducted to investigate the effect of radius, gas flow velocity, and stretch rate on the flame spread and extinction behavior. The major conclusions are drawn as follows:

(1) The horizontal flame spread rate at the bottom surface increases with the flow velocity but decreased with radius when $X_{O2} \geq$ 21%, while the spread rate appears less sensitive to the variation of flow velocity and radius near the extinction limit conditions ($X_{O2} = 18\%$).
(2) The flame spread rate can be correlated by the stretch rate for flame spread over samples with different diameters under different flow velocities. The scaling analysis neglecting surface radiation and curvature effect shows that the flame spread rates are approximately in proportion to the square root of the stretch rate.
(3) Flame extinction is dominated by stretch rate and solid-phase heat loss. The smaller cylinder can sustain burning at a lower oxygen concentration due to the less solid-phase heat loss.

CRediT authorship contribution statement

Chuanjia Wu: Investigation, Methodology, Writing – original draft. **Feng Zhu:** Conceptualization, Supervision, Project administration, Writing – review & editing. **Shuangfeng Wang:** Investigation, Project administration, Writing – review & editing.

Declaration of competing interest

The authors declare that they have no known competing financial interests or personal relationships that could have appeared to influence the work reported in this paper.

Acknowledgments

Funding was provided by the National Key R&D Program of China under Grant No. 2021YFA0716203, the Opening Fund of State Key Laboratory of Fire Science (SKLFS) under Grant No. HZ2021-KF12, and the National Natural Science Foundation of China under Grant No. U1738117.

Appendix

The velocity profile at 15 mm above the outlet of the flow tunnel is shown in Figure A1. The gas flow velocity near the wall is slightly slower about 2 – 5 cm/s than that in the central region mainly due to the effect of the boundary layer. The average velocity is close to the forced flow velocity Vg. In general, it can be considered that the flow field around the sample is uniform.

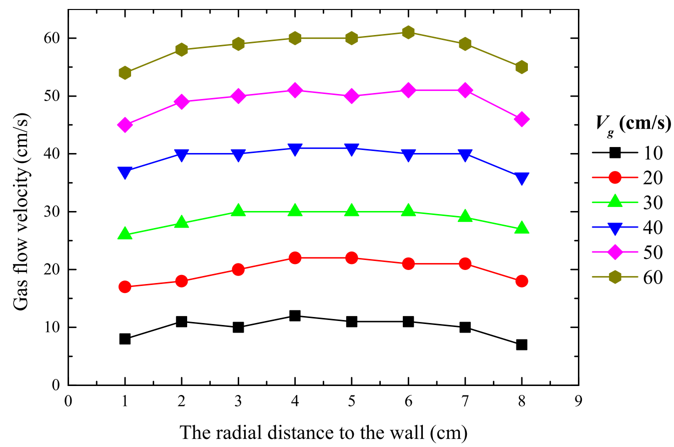

Fig. A1. The velocity profile above the flow tunnel at different forced flow velocities.

The position of the flame leading edge at the bottom surface of the PMMA cylinders as a function of time is measured at various oxygen concentrations and sample radii as shown in Figure A2. It is seen that the flame leading edge position has a linear relationship with time. Therefore, the horizontal flame spread at an upward forced flow environment is in a steady state.

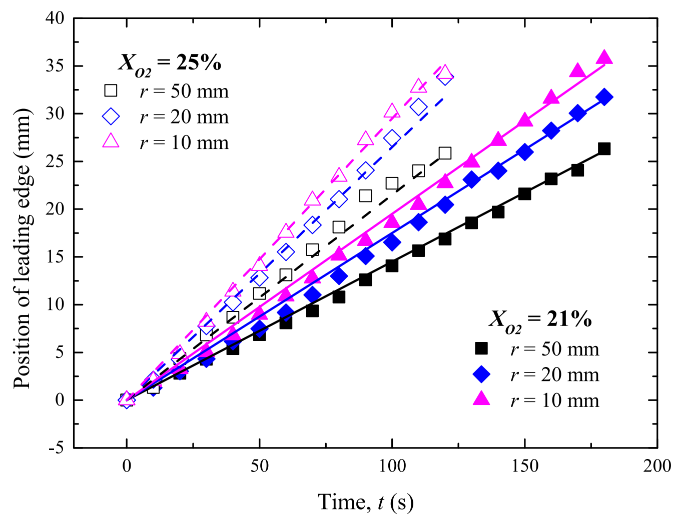

Fig. A2. The time evolution of flame leading-edge position for three PMMA cylinders at Vg = 10 cm/s and X_{O2} = 21%, 25%.

References

[1] A.C. Fernandez-Pello, The solid phase, in: Combust. Fundam. Fire, 1995, pp. 31–100.

[2] A.C. Fernandez-Pello, T. Hirano, Controlling mechanisms of flame spread, Combust. Sci. Technol. 32 (1983) 1–31, https://doi.org/10.1080/00102208308923650.

[3] J.G. Quintiere, Fundamentals of Fire Phenomena, John Wiley & Sons, 2006, https://doi.org/10.1002/0470091150.

[4] M.J. Gollner, C.H. Miller, W. Tang, A.V. Singh, The effect of flow and geometry on concurrent flame spread, Fire Saf. J. 91 (2017) 68–78, https://doi.org/10.1016/j.firesaf.2017.05.007.

[5] M.J. Gollner, X. Huang, J. Cobian, A.S. Rangwala, F.A. Williams, Experimental study of upward flame spread of an inclined fuel surface, Proc. Combust. Inst. 34 (2013) 2531–2538, https://doi.org/10.1016/j.proci.2012.06.063.

[6] M. Sibulkjn, C.K. Lee, Flame propagation measurements and energy feedback analysis for burning cylinders, Combust. Sci. Technol. 9 (1974) 137–147, https://doi.org/10.1080/00102207408960349.

[7] A. Ito, T. Kashiwagi, Characterization of flame spread over PMMA using holographic interferometry sample orientation effects, Combust. Flame 71 (1988) 189–204, https://doi.org/10.1016/0010-2180(88)90007-7.

[8] X. Chen, J. Liu, Z. Zhou, P. Li, T. Zhou, D. Zhou, J. Wang, Experimental and theoretical analysis on lateral flame spread over inclined PMMA surface, Int. J. Heat Mass Tran. 91 (2015) 68–76, https://doi.org/10.1016/j.ijheatmasstransfer.2015.07.072.

[9] R. Tu, X. Ma, Y. Zeng, X. Zhou, L. He, T. Fang, J. Fang, Coupling effects of pressure and inclination on downward flame spread over flexible polyurethane foam board, Build. Environ. 164 (2019), https://doi.org/10.1016/j.buildenv.2019.106339.

[10] L. Zhou, A.C. Fernandez-Pello, Turbulent, concurrent, ceiling flame spread: the effect of buoyancy, Combust. Flame 92 (1993) 45–59, https://doi.org/10.1016/0010-2180(93)90197-B.

[11] J. de Ris, L. Orloff, The role of buoyancy direction and radiation in turbulent diffusion flames on surfaces, Symp. Combust. 15 (1975) 175–182, https://doi.org/10.1016/S0082-0784(75)80295-5.

[12] J.M. Tizón, J.J. Salvá, A. Liñán, Wind-aided flame spread under oblique forced flow, Combust. Flame 119 (1999) 41–55, https://doi.org/10.1016/S0010-2180(99)00038-3.

[13] K. Zhao, M.J. Gollner, Q. Liu, J. Gong, L. Yang, Lateral flame spread over PMMA under forced air flow, Fire Technol 56 (2020) 801–820, https://doi.org/10.1007/s10694-019-00904-x.

[14] F. Higuera, A. Liñán, Flame spread along a fuel rod in the absence of gravity, Combust. Theor. Model. 3 (1999) 259–265, https://doi.org/10.1088/1364-7830/3/2/003.

[15] F.J. Higuera, Flame spread along thermally thick horizontal rods, Combust. Theor. Model. 6 (2002) 197–208, https://doi.org/10.1088/1364-7830/6/2/303.

[16] F.J. Higuera, Flame spread along horizontal solid fuel cylinders, Proc. Combust. Inst. 29 (2002) 211–217, https://doi.org/10.1016/S1540-7489(02)80029-3.

[17] D.W. Foutch, J.S. T'ien, Extinction of a stagnation-point diffusion flame at reduced gravity, AIAA J 25 (1987) 972–976, https://doi.org/10.2514/3.9730.

[18] J.B. Armstrong, S.L. Olson, J.S. T'ien, Transient model and experimental validation of low-stretch solid-fuel flame extinction and stabilization in response to a step

change in gravity, Combust. Flame 147 (2006) 262–277, https://doi.org/10.1016/j.combustflame.2006.09.007.
[19] S.L. Olson, J.S. T'ien, Buoyant low-stretch diffusion flames beneath cylindrical PMMA samples, Combust. Flame 121 (2000) 439–452, https://doi.org/10.1016/S0010-2180(99)00161-3.
[20] M.C. Johnston, J.S. T'ien, Gravimetric measurement of solid and liquid fuel burning rate near and at the low oxygen extinction limit, Fire Saf. J. 91 (2017) 140–146, https://doi.org/10.1016/j.firesaf.2017.03.027.
[21] I.S. Wichman, Flame spread in an opposed flow with a linear velocity gradient, Combust. Flame 50 (1983) 287–304, https://doi.org/10.1016/0010-2180(83)90071-8.
[22] S. Hossain, I.S. Wichman, F.J. Miller, S.L. Olson, Opposed flow flame spread over thermally thick solid fuels: buoyant flow suppression, stretch rate theory, and the regressive burning regime, Combust. Flame 219 (2020) 57–69, https://doi.org/10.1016/j.combustflame.2020.05.001.
[23] A.C. Fernandez-Pello, S.R. Ray, I. Glassman, Flame spread in an opposed forced flow: the effect of ambient oxygen concentration, Symp. Combust. 18 (1981) 579–589, https://doi.org/10.1016/S0082-0784(81)80063-X.
[24] C. Wu, X. Huang, S. Wang, F. Zhu, Y. Yin, Opposed flame spread over cylindrical PMMA under oxygen-enriched microgravity environment, Fire Technol 56 (2020) 71–89, https://doi.org/10.1007/s10694-019-00896-8.
[25] C. Wu, F. Zhu, S. Wang, Experimental study on flame spread over cylindrical solid fuels in micro and normal-gravity environments, J. Eng. Thermophys. 40 (2019) 2672–2677.
[26] M.A. Delichatsios, R.A. Altenkirch, M.F. Bundy, S. Bhattacharjee, L. Tang, K. Sacksteder, Creeping flame spread along fuel cylinders in forced and natural flows and microgravity, Proc. Combust. Inst. 28 (2000) 2835–2842, https://doi.org/10.1016/S0082-0784(00)80706-7.
[27] X. Huang, S. Link, A. Rodriguez, M. Thomsen, S. Olson, P. Ferkul, C. Fernandez-Pello, Transition from opposed flame spread to fuel regression and blow off: effect of flow, atmosphere, and microgravity, Proc. Combust. Inst. 37 (2019) 4117–4126, https://doi.org/10.1016/j.proci.2018.06.022.
[28] F.A. Williams, Combustion Theory, second ed., 1985, https://doi.org/10.1201/9780429494055.
[29] J.N. De Ris, Spread of a laminar diffusion flame, Symp. Combust. 12 (1969) 241–252, https://doi.org/10.1016/S0082-0784(69)80407-8.
[30] S. Tao, J. Fang, L. Zhao, J. Wang, H.R. Shah, L. Hu, L. Yang, Flammability and critical parameters at low oxygen extinction limit of stagnation-point diffusion flames with varied stretch rates, Fire Saf. J. 116 (2020) 103203, https://doi.org/10.1016/j.firesaf.2020.103203.
[31] S. Bhattacharjee, K. Wakai, S. Takahashi, Predictions of a critical fuel thickness for flame extinction in a quiescent microgravity environment, Combust. Flame 132 (2003) 523–532, https://doi.org/10.1016/S0010-2180(02)00501-1.
[32] S.L. Olson, P.V. Ferkul, Microgravity flammability boundary for PMMA rods in axial stagnation flow: experimental results and energy balance analyses, Combust. Flame 180 (2017) 217–229, https://doi.org/10.1016/j.combustflame.2017.03.001.
[33] C. Wu, P. Sun, X. Wang, X. Huang, S. Wang, Flame extinction of spherical PMMA in microgravity: effect of fuel diameter and conduction, Microgravity Sci. Technol. 32 (2020) 1065–1075, https://doi.org/10.1007/s12217-020-09829-5.
[34] C.T. Yang, J.S. T'ien, Numerical simulation of combustion and extinction of a solid cylinder in low-speed cross flow, J. Heat Tran. 120 (1998) 1055–1063, https://doi.org/10.1115/1.2825890.